OCEAN APPLICATIONS TECHNICAL NOTE 19

Validation of Ocean Heat Transport in Had CM2.

by

H T Banks.

Met Office
FitzRoy Road, Exeter, Devon. EX1 3PB

Met Office
FitzRoy Road, Exeter, Devon. EX1 3PB

1 Introduction

At the top of the atmosphere, heat is gained in tropical regions and lost near the poles. This pattern implies that the combined ocean-atmosphere system must transport heat polewards. A long debate has existed between meteorologists and oceanographers regarding whether this transport of heat is produced mainly by the atmosphere or by the ocean.

In order to address this question, oceanographers have collected data from transoceanic zonal sections. This has enabled estimates to be made both of the total ocean heat transport across any section and also the mechanisms which produce the heat transport. The mechanisms of ocean heat transport are able to tell us something about the circulation which can then be combined with estimates of the mass transport across the section. A robust test for ocean models employed in climate simulations is to examine the mechanisms producing transport of heat and to compare with estimates from hydrography. This method assists with validating the ocean circulation and in the diagnosis of the systematic model errors.

There are two other reasons why such intercomparison studies are useful; firstly, direct comparisons between model results and hydrographic sections allow us to test the assumptions which are employed when a section is 'worked up' to provide estimates of heat transport and secondly, the divergence of ocean heat transport must be equal to the surface heat flux. Hence, examining the ocean heat transport also gives us information about the fluxes which drive the ocean model in a coupled ocean-atmosphere model. In what will follow, we first review the method used by hydrographers when analysing sections and define the method we employ to calculate the components of the heat transport from the model to allow us to make a comparison with observations. We then examine in detail the results from the coupled ocean-atmosphere model HadCM2 (see Johns *et al* (1997) for details) at the end of the spin-up phase.

2 Calculating ocean heat transport

Northward heat transport, Π, across any section is defined as:

$$\Pi = \int \int \rho_0 C_p v \theta dz dx \tag{1}$$

where ρ_0 is the reference density, C_p is the specific heat capacity of seawater at constant pressure, v is the meridional velocity (directed northward) and θ is the potential temperature. Formally, this is only a well-defined quantity if the mass transport across the section is identical to zero, i.e.

$$\psi = \int \int v dz dx = 0 \tag{2}$$

since if mass is not conserved the value of the heat transport would be changed by an adjustment of the temperature scale. However, in practice, some sections have a non-zero mass flux across them and interpreting the sections can be difficult. We will return to this issue later.

In the manner of Hall and Bryden (1982) we rewrite the heat transport as the sum of its components:

$$\Pi = \int \int \rho_0 C_p v_{wbc} \theta dz dx + \int \int \rho_0 C_p v_{ekman} \theta dz dx + \int \int \rho_0 C_p v_{int} \theta dz dx \tag{3}$$

where *wbc* is the western boundary current contribution, *ekman* is the Ekman layer contribution and *int* is the interior contribution. It should be noted that individually each term on the right-hand side of equation (3) represents a temperature transport (rescaled to the units of a heat flux) since each term has a non-zero mass transport.

In what follows we will describe both how these terms are estimated given a hydrographic section (requiring a further breakdown of the terms which we will describe) and also the procedure for deducing the terms from the model fields in such a way to allow maximum comparison between the model and observations. Essentially, we wish to treat the model fields as observations (in as far as possible) and make a meaningful comparison between the model components of the heat transport and the observational estimates of the components. To allow this we also consider only the *advective* heat transport (ie, that which is given by the advection of temperature) and ignore the diffusive heat transport (ie, that given by the diffusive parameterisations in the model) since this has the most direct correspondence with the observational estimates. We should also note that in many parts of the ocean model the diffusive heat transport is small compared with the advective heat transport.

2.1 Western boundary current

From hydrographic sections, velocity measurements in the western boundary current generally derive from high resolution Acoustic Doppler Current Profiler (ADCP) measurements, so exact velocities are known. We consider the model velocities to be comparable in this sense to the hydrographic measurements (ie, velocities in the western boundary current are known exactly). It is sometimes convenient to divide the velocity, v, and the potential temperature, θ, profiles into their barotropic ($\overline{v}$, $\overline{\theta}$) and baroclinic (v', θ') components. $\overline{v}(x, y)$ is given by:

$$\frac{1}{H}\int_0^H v(x,y,z)dz$$

where H is the depth of the ocean at position (x,y) and $v'(x,y,z)$ is given by:

$$v(x,y,z) - \overline{v}(x,y).$$

Then the western boundary contribution is defined via:

$$\int\int \rho_0 C_p v_{wbc}\theta dzdx = \int\int \rho_0 C_p \overline{v_{wbc}}\overline{\theta}dzdx + \int\int \rho_0 C_p v'_{wbc}\theta' dzdx \quad (4)$$

$$\equiv \rho_0 C_p \psi_{wbc}\tilde{\theta}_{wbc} + \int\int \rho_0 C_p v'_{wbc}\theta' dzdx \quad (5)$$

where ψ_{wbc} is the total transport of the western boundary current and is given by:

$$\psi_{wbc} = \int\int v_{wbc}dzdx$$

and $\tilde{\theta}_{wbc}$ denotes the transport-weighted temperature across the western boundary current and is given by:

$$\tilde{\theta}_{wbc} = \frac{\left(\int\int \overline{v_{wbc}}\overline{\theta}dzdx\right)}{\psi_{wbc}}.$$

The first term of equation (5) denotes the temperature transported by the barotropic flow in the western boundary current (since the mass transport is non-zero) and the second term denotes the heat transported by the baroclinic flow in the western boundary current (with a zero net mass transport).

In the model, the division between the interior and the western boundary current may be somewhat 'blurred'. This problem is greatest when the resolution is coarse and the horizontal viscosity is high. The calculation of the various components of the heat transport is dependent therefore on the particular choice of where these divisions should lie, although in practice, we define the western boundary current edge as the point at which the mass transport is maximised from the western boundary. The western boundary current in the model has a width of O(20 degrees of longitude) which is greater than the observed width of O(< 5 degrees of longitude). Across some model sections (in this analysis the 24°N section in the Atlantic), there is a strong deep western boundary current flowing below the western boundary current and in the opposite direction (because of the width of the western boundary current). When this is the case, the

mass and heat transported by the deep western boundary current in the model is included in the analysis as part of the interior return flow. In observational studies the geographical definition of the sections usually ensures that the deep western boundary current falls within the interior of the hydrographic section. A careful definition of the boundary currents is required to provide any meaning to a comparison with observations.

2.2 Ekman layer

Across hydrographic sections, observationalists estimate the Ekman transport using climatological windstress fields. Given the observed zonal windstress, τ_x, for the mid-ocean, the northward Ekman transport, ψ_{ekman}, is approximated by:

$$\psi_{ekman} = \int\int v_{ekman} dx dz = \int \frac{-\tau_x}{\rho_0 f} dx \tag{6}$$

where f is the Coriolis parameter.

To estimate the Ekman heat transport, Hall and Bryden (1982) assumed that the Ekman layer was 50 m deep with Ekman velocities decreasing linearly to zero at 50 m. The Ekman layer temperature (θ_{ekman}) was prescribed to be a weighted average of the surface temperature (θ_0) and the temperature at 50 m (θ_{50}), such that $\theta_{ekman} = (2\theta_0 + \theta_{50})/3$. Then the Ekman layer temperature transport (since the mass transport is non-zero) can be estimated from:

$$\int\int \rho_0 C_p v_{ekman} \theta dz dx = \int C_p \frac{-\tau_x}{f} \theta_{ekman} dx \equiv \rho_0 C_p \psi_{ekman} \tilde{\theta}_{ekman} \tag{7}$$

where $\tilde{\theta}_{ekman}$ is the transport-weighted temperature in the Ekman layer given by:

$$\tilde{\theta}_{ekman} = \frac{\left(\int \frac{-\tau_x}{f} \theta_{ekman} dx\right)}{\rho_0 \psi_{ekman}}.$$

In the model we must deduce the Ekman velocities away from the western boundary current, $v_{ekman}(x, z)$. This allows us to calculate the centre of equation (6) directly and compare with the right-hand side of equation (6), which represents the observational estimate. The Ekman velocity, v_{ekman}, is given by:

$$v_{ekman} = v - v_g \tag{8}$$

where v is the absolute velocity (i.e. the model velocity) and v_g is the geostrophic velocity which is calculated from the thermal wind equation assuming a matching level at the base of the Ekman

layer[1]. By definition, the Ekman velocity, v_{ekman}, is the ageostrophic velocity in the surface layer but we refrain from using this definition since we are only considering the surface layer. The Ekman velocity is illustrated in figure 1; the model velocity profile is shown by the bold line while the geostrophic velocity profile (calculated from the model density) is shown by the dashed line. The geostrophic velocity has been matched to the model velocity at 50 m since below 50 m the shape of the curves are very similar and it is only at shallower depths, in the Ekman layer, that significant departures from geostrophy are apparent. In the model, the base of the Ekman layer is chosen to be that depth which maximises the agreement between the estimates of the mass transport from the velocities and that from the windstresses (c.f. equation (6)) and is usually at approximately 50 metres (or model level 4).

2.3 Interior

The interior heat transport can be written as the sum of its barotropic and baroclinic components:

$$\int\int \rho_0 C_p v_{int} \theta dz dx = \int\int \rho_0 C_p \overline{v_{int}}\overline{\theta} dz dx + \int\int \rho_0 C_p v'_{int} \theta' dz dx. \tag{9}$$

For the model, v_{int} is defined as the absolute model velocity, v, minus the Ekman velocity, v_{ekman} (if ageostrophic flow only exists in the Ekman layer then $v_{int} = v_g$ from equation (8)). The first term on the right-hand side of equation (9) describes the temperature transported by the interior barotropic flow. The barotropic component can be divided into two parts corresponding to the compensation in terms of mass transport of the Ekman and western boundary current components, i.e.,

$$\int\int \rho_0 C_p \overline{v_{int}}\overline{\theta} dz dx \equiv -\rho_0 C_p \tilde{\theta}_{int} (\psi_{ekman} + \psi_{wbc}) \tag{10}$$

where $\tilde{\theta}_{int}$ denotes a section average potential temperature and is given by:

$$\tilde{\theta}_{int} = \frac{\left(\int\int \overline{v_{int}}\overline{\theta} dz dx\right)}{\psi_{int}}$$

and $\psi_{int} = -(\psi_{wbc} + \psi_{ekman})$ (so that the total section has a zero net mass transport). The second term on the right-hand side of equation (9) describes the heat transported by the interior baroclinic flow (since the net mass transport is zero).

For the hydrographic sections, v'_{int}, is defined as the geostrophic velocity referenced to an arbitrary reference level (although in practice is usually chosen such that the baroclinic circulation

[1]We can choose the level of no motion to be at any depth and match the geostrophic and model velocities at the base of the Ekman layer by adding a barotropic velocity.

is consistent with the water masses and preconceived notions of the circulation). The barotropic velocities $\overline{v_{int}}$ are generally unknown from the hydrography (although sometimes ADCP velocities can be used to infer the barotropic velocities) but, given the net volume transport by the western boundary current and the Ekman layer (so ψ_{int} is known) and an estimate of $\tilde{\theta}_{int}$ (by making the assumption that $\overline{\theta}$ is independent of the x-direction and taking it outside the integral on the LHS of equation (10)), the barotropic components of the interior heat transport can be estimated for observational studies.

2.4 Component contributions

In this section we will summarise the breakdown of the total heat transport into the various components which are traditionally employed by observationalists and then organise the terms so that the total heat transport can be described in terms of an Ekman, interior and western boundary current component. In the previous section we described how the barotropic interior transport can be divided between the western boundary current and Ekman components and we use this here to define three major components each with a net mass transport of zero. Starting from equation (3) and using equations (5), (7), (9) and (10), the heat transport across the section can be written as:

$$\begin{aligned}\Pi \;=\; & \overbrace{\rho_0 C_p \psi_{wbc}\tilde{\theta}_{wbc}}^{a} \overbrace{+\rho_0 C_p \int\int v'_{wbc}\theta' dzdx}^{b} \\ & \overbrace{+\rho_0 C_p \psi_{ekman}\tilde{\theta}_{ekman}}^{c} \overbrace{+\int\int \rho_0 C_p v'_{int}\theta' dzdx}^{d} \\ & \underbrace{-\rho_0 C_p \psi_{wbc}\tilde{\theta}_{int}}_{e} \underbrace{-\rho_0 C_p \psi_{ekman}\tilde{\theta}_{int}}_{f}\end{aligned} \tag{11}$$

Then rearranging, such that the barotropic temperature transport component of the interior (terms e and f in equation (11) and often referred to as the compensation terms) is grouped with the western boundary current and Ekman component (respectively), we obtain:

$$\begin{aligned}\Pi \;=\; & \overbrace{\rho_0 C_p \left(\int\int v'_{wbc}\theta' dzdx + \Delta\theta_{wbc}\psi_{wbc}\right)}^{A=b+a+c} + \overbrace{\rho_0 C_p \Delta\theta_{ekman}\psi_{ekman}}^{B=c+f} \\ & + \overbrace{\int\int \rho_0 C_p v'_{int}\theta' dzdx}^{C=d}\end{aligned} \tag{12}$$

where $\Delta\theta_{wbc}$ (= $\tilde{\theta}_{wbc}$ - $\tilde{\theta}_{int}$) and $\Delta\theta_{ekman}$ (= $\tilde{\theta}_{ekman}$ - $\tilde{\theta}_{int}$) are the transport-weighted temperature

differences of the western boundary current and Ekman layer respectively. This ensures that each component has a well-defined heat transport (rather than a temperature transport which has a more dubious interpretation). When summarising the components of the heat transport we will nominally refer to the first term (A) on the right-hand side of equation (12) as the western boundary current contribution, the second term (B) as the Ekman component and the third term (C) as the interior contribution.

Gyre and overturning contributions

Finally, we can estimate the relative contributions to the meridional heat flux from the meridional-vertical overturning and from the horizontal circulation cell. The overturning contribution can be written:

$$\rho_0 C_p \int < v(z) >< \theta(z) > L(z) dz \tag{13}$$

where $< >$ indicate zonal averages and $L(z)$ is the basin width at any depth, and the horizontal circulation contribution can be written:

$$\rho_0 C_p \int \int (v - < v >)(\theta - < \theta >) dx dz. \tag{14}$$

3 Comparison of observations and model results

3.1 Global results

Figure 2 shows a compilation of some of the most recent observational estimates of ocean heat transport; HB denotes Hall and Bryden (1982), BRC denotes Bryden *et al* (1991), MW denotes Macdonald and Wunsch (1996), TBB denotes Tsimplis *et al* (1996), Fu is Fu (1981), R is Rintoul (1991), TW is Toole and Warren (1993) and SK is Saunders and King (1995). Figure 3 shows the heat transport across the latitude circles for HadCM2 calculated for the 5 year mean at the end of the spin-up phase. While the pattern of heat transport is generally in good agreement, there are regions which are notably at odds with the observations (in particular, the South Pacific). At 24°N, the magnitude of heat transport is generally smaller than observed/estimated values but in the right direction everywhere. At 47°N the heat transport in the Atlantic is smaller than that estimated by Macdonald and Wunsch (1996), while in the Pacific the (small) net heat transport is in the opposite direction to their value. In the South Atlantic, the heat transport in HadCM2 is in remarkable agreement with the observations. In the Indo-Pacific region, there is a net mass

transport across the sections due to the Indonesian throughflow. In these cases the heat transport values are actually temperature transports and there is some difficulty comparing these values with observations especially since the magnitude of the Indonesian throughflow (23.0 Sv) lies outside the observational range of 0-20 Sv Wijffels *et al* (1996). Tsimplis *et al* (1996) employed a value of 0 Sv for the magnitude of the Indonesian throughflow in their estimates while Macdonald and Wunsch (1996) employed a value of 9 Sv and Toole and Warren (1993) employed a value of 6.7 Sv.

In what follows we will compare the model results in detail with the observations for the North Atlantic, North Pacific, South Atlantic, South Pacific and Indian Ocean. In the Northern oceans at 24°N, estimates from observations are believed to be robust, while in the Southern hemisphere oceans at a latitude of approximately 30°S, current hydrographic results show large variations.

3.2 Atlantic 24°N

Figure 4 shows the 24°N section. For this section we have split the western boundary current (WBC) into two parts; a western section in the Gulf of Mexico and a section to the east of this which only extends down to 666 m. Below the eastern section is the deep western boundary current (DWBC) which is included in the interior contribution. Although this type of separation is not made in the observations, if we did not separate the northward flowing WBC from the southward flowing DWBC any comparison between the model and observations would be meaningless. It is impossible to define barotropic and baroclinic components for the eastern section of the WBC and the DWBC (since neither extends to full depth) so we treat them only as barotropic components.

The results for the components of the northward heat transport in HadCM2 are shown in table 1, which is equivalent to table 1 of Hall and Bryden (1982). The relationship of the terms to those given in equation (11) is marked. Below the magnitude of the heat transport we have described many of the terms as equivalent to a volume transport multiplied by a temperature. The equivalent temperatures are derived by dividing the heat transport of a component by the volume transport of that component, the specific heat capacity and the reference density. The Ekman component is given by the model derived Ekman velocities. For this section the difference between the Ekman temperature transport from the model velocities and the estimate from the windstress is 0.01 PW. The components are summarised and compared with the estimates of Hall and Bryden (1982) in table 2 (the relationship of the components to those given in equation (12) is marked). At first glance the model appears to be doing reasonably well at simulating the heat transport. However, the definition of such a broad WBC lies uneasily within the framework of the observations since observations show a WBC with a width of a few degrees. The results highlight several discrepancies

Component	Barotropic	Baroclinic	Ekman	Total
WBC (west) WBC (east)	0.27 (a) 2.09 (a) 36.3 Sv @ 15.8°C	0.29 (b)	-	2.65 = 36.3 @ 17.8°C (a+b)
DWBC	-0.50 (e) -22.5 Sv @ 5.4°C			
Interior Geostrophic		-1.18 (d)	0.29 (c) 3.0 Sv @ 23.6°C	-1.80 = 36.3 Sv @ 12.0°C (c+d+e+f)
Compensation	-0.34 (e) -13.8 Sv @ 6.0°C		-0.07 (f) -3.0 Sv @ 5.7°C	
Total	1.52 (a+e) 36.3 Sv @ $\Delta\theta = 10.2$°C	-0.89 (b+d)	0.22 (c+f) 3.0 Sv @ $\Delta\theta = 17.9$°C	0.85

Table 1: Northward heat transport in HadCM2 across 24°N in the Atlantic. Units are PW (= 10^{15} W). The table is almost comparable to table 1 from Hall and Bryden (1982). The relationship of the components to those identified in equation (11) is marked.

Component	HadCM2	Observations
WBC (A = b+a+e)	1.81 PW = 36.3 Sv @ $\Delta\theta = 12.2$°C	1.73 PW = 29.5 Sv @ $\Delta\theta = 14.3$°C
Interior (C = d)	-1.18 PW	-0.93 PW
Ekman (B = c+f)	0.22 PW = 3.0 Sv @ $\Delta\theta = 18.7$°C	0.42 PW = 5.0 Sv @ $\Delta\theta = 20.5$°C
Total (A+B+C)	0.85 PW	1.22 PW

Table 2: A summary of the components of the northward heat transport across 24°N in the Atlantic from HadCM2 and from observational estimates. The relationship of the terms to those given in equation (12) is marked.

between the model and the real ocean: the Ekman heat transport is almost a factor of two too small, a result of the Ekman layer being both too cold and having a volume transport which is too small (reflecting weaker integrated windstresses). The WBC is also too cold (partly due to the fact that it is so smeared out), while the southward return flow transports too much heat southward, as a result of being several degrees too warm.

This last point is emphasised if we look at the transport of the interior and the WBC in temperature classes, as shown in table 3. We see that in the observations most of the return flow takes place at temperatures less than 4°C, while in the model most of the southward return flow of North Atlantic Deep Water (NADW) takes place at temperatures between 4°C and 7°C. Below 4°C in the model, the transport is northward. Northward flow at this temperature represents the transport of Antarctic Bottom Water (AABW), which is observed in the hydrographic section but at much deeper, colder levels.

Temperature class		WBC transport	Interior + Ekman transport	Total transport
$\theta > 17°C$	model	19.5	-10.8	8.7
	obs	18.4	-9.5	8.9
$12°C < \theta < 17°C$	model	6.9	-8.1	-1.2
	obs	5.4	-2.9	2.5
$7°C < \theta < 12°C$	model	9.8	-0.2	9.6
	obs	4.7	1.9	6.6
$4°C < \theta < 7°C$	model	0.2	-18.6	-18.4
	obs	1.0	-3.3	-2.3
$\theta < 4°C$	model	-	1.3	1.3
	obs	-	-15.6	-15.6

Table 3: Northward volume transport across 24°N in the Atlantic in temperature classes. Units are Sv (= 10^6 m^3 s^{-1}). The top line for each temperature class shows the model transport. The bottom line shows the observed transport.

Table 4 shows the transport in depth classes in HadCM2 along with the average temperature for that class. The classes chosen by Hall and Bryden (1982) differ from the model depths. Figure 5 shows the transport per unit depth for the model and for the observations. In each case, the dashed line indicates the WBC and the solid line indicates the interior plus Ekman contribution. Hall and Bryden (1982) show the southward flow extending down to 5500m while in HadCM2 it is largely confined to depths shallower than 3000m. In the model, the southward flow of NADW is both too warm (as illustrated by figure 5) and too shallow. The formation of NADW in the model is particularly sensitive to the overflows across the Greenland-Iceland-Scotland ridge (Roberts *et al*, 1996).

In HadCM2 the heat transport across 24°N in the Atlantic comprises of 0.76 PW due to the meridional overturning and 0.09 PW due to the horizontal circulation. This should be compared with 1.28 PW by the overturning and -0.06 PW by the horizontal circulation for the observations.

3.3 Pacific 24°N

For this section, the distinction between the WBC and the interior is much clearer (as shown by the slopes of the isotherms on figure 4) and allows better comparison with the estimates made from observations by Bryden *et al* (1991). The WBC is defined to have a width comparable with that employed in the previous section (18.75°in this case) but now there is only one branch of the WBC. The same procedure for calculating the components of the heat transport is carried out as described above for the Atlantic section. The results are summarised in tables 5 and 6. The results are presented in a similar manner to those for the Atlantic section which is equivalent to

Model depth	WBC transport	WBC temperature	Interior + Ekman transport	Interior temperature
5	1.724	26.498	0.744	23.489
15	1.192	26.494	0.394	23.488
25	0.804	26.462	-0.177	23.475
35	0.681	26.273	-0.486	23.439
48	0.960	25.721	-0.812	23.285
67	1.422	24.953	-1.068	22.676
96	2.062	23.944	-1.435	21.704
139	1.859	22.553	-2.013	20.822
204	3.776	20.022	-2.990	19.258
301	6.270	16.238	-4.138	16.975
447	7.972	12.648	-4.277	14.969
666	6.510	9.995	-2.627	12.957
996	1.171	7.821	-0.192	9.802
1500			-6.938	6.150
2120			-8.139	4.001
2730			-3.147	3.185
3350			-1.012	1.637
3960			-0.787	1.088
4580			1.021	0.927
5190			0.992	0.656

Table 4: Northward volume transport in HadCM2 across 24°N in the Atlantic in depth classes. Units are Sv (= 10^6 m^3 s^{-1}) and °C.

Component	Barotropic	Baroclinic	Ekman	Total
WBC	0.65 (a) 31.2 Sv @ 5.1°C	1.60 (b)	-	2.25 = 31.2 Sv @ 17.6°C (a+b)
Interior Geostrophic		-2.31 (d)	1.07 (c) 10.7 Sv @ 24.4°C	-1.96 = 31.2 Sv @ 15.3°C
Compensation	-0.54 (e) -31.2 Sv @ 4.2°C		-0.18 (f) -10.7 Sv @ 4.2°C	(c+d+e+f)
Total	0.11 (a+e) 31.2 Sv @ $\Delta\theta = 0.9$°C	-0.71 (b+d)	0.89 (c+f) 10.7 Sv @ $\Delta\theta = 20.3$°C	0.29

Table 5: Northward heat transport in HadCM2 across 24°N in the Pacific. Units are PW (= 10^{15} W). The relationship of the components to those given in equation (11) is marked.

Component	HadCM2	Observations
WBC (A = b+a+e)	1.71 PW = 31.2 Sv @ $\Delta\theta = 13.4$°C	1.73 PW = 28.3 Sv @ $\Delta\theta = 14.9$°C
Interior (C = d)	-2.31 PW	-1.91 PW
Ekman (B = c+f)	0.89 PW = 10.7 Sv @ $\Delta\theta = 20.3$°C	0.93 PW = 12.0 Sv @ $\Delta\theta = 19.0$°C
Total (A+B+C)	0.29 PW	0.75 PW

Table 6: Summary of the components of the northward heat transport across 24°N in the Pacific from HadCM2 and from observations. The relationship of the components to those given in equation (12) is marked.

method 2 of Bryden *et al* (1991) which they argue is the method which is most representative of the three-dimensional circulation. For this section the difference between calculating the Ekman heat transport from the model velocities and making an estimate from the model windstresses is 0.10 PW (giving an increase of 10% using the model windstresses).

Table 6 suggests that there are several reasons for the discrepancies between the model and observed heat transport in a much clearer manner than was possible for the previous section. The Ekman transport introduces a small error (0.04 PW) but is not the major source of the model error. The WBC in the model appears to transport heat through a baroclinic rather than barotropic flow which is incompatible with the observed split (the model transports 0.11 PW northward barotropically (term (a+e) in equation (11)) and 1.60 PW baroclinically (term (b) in equation (11)), while the observational estimate of Bryden *et al* (1991) consists of 0.85 PW transported barotropically and 0.88 PW transported baroclinically), but the model does get approximately the right WBC heat and mass transport (31.2 Sv c.f. 28.3 Sv in table 6). The major source of error however, is the interior return flow. The baroclinic interior heat transport is overestimated

in the model by 0.4 PW while the return flow for the WBC (represented by terms c+d+e+f) is approximately 3°C too warm (15.3°C c.f. 11.7°C) in the model. In fact, it is noteworthy that if the temperatures of the return flow were replaced by the observed temperatures, for both of the sections at 24°N the heat transport would be correct to an accuracy greater than 0.1 PW. The spreading of the thermocline (as shown in figure 4), which leads to warming at deeper levels, appears to be the most likely candidate for this problem. The spreading of the thermocline is a widespread problem with Cox models. This problem also exists in the Atlantic but is secondary to the problem of the return flow of NADW.

The estimate of 0.75 PW of the total heat transport from observations comprises of 0.38 PW from the gyre contribution and 0.38 PW from the overturning contribution. In HadCM2, the total heat transport of 0.29 PW is almost entirely due to the overturning circulation with just 0.08 PW due to the horizontal circulation.

3.4 South Atlantic

In the South Atlantic, the ocean heat transport is northward (contrary to the usual assumption that heat is transported poleward everywhere). At 30°S, Fu (1981) estimates 0.8 PW northward, Rintoul (1991) estimates 0.25 PW and Macdonald and Wunsch (1996) estimated 0.5 PW. The model heat flux of 0.44 PW lies comfortably between these values. All of these estimates derive from inverse calculations. The calculation of the heat transport from the inverse method does not usually split the heat transport in the same manner as Hall and Bryden (1982) and the comparison is usually more limited than the 24°N sections.

To enable a more detailed comparison, the heat transport across WOCE section A11 has been calculated. The WOCE A11 hydrographic section is marked on figure 3. Since the section is not entirely zonal calculations are made more complicated. The 'northward' transport is taken to be that from the southern to the northern side of the section. The results from the model and the observations (Saunders and King, 1995) are summarised in table 7. The Ekman transport and the total heat transport agree well with the observations of Saunders and King (1995) though the WBC mass transport is significantly underestimated in the model. Figure 6 shows the mass transport, as a function of depth, integrated for the whole section and compared with the results of Saunders and King (1995) for two of their solutions; the dotted line denotes the preferred solution (this is the solution used in their paper and represents climatology), while the dashed line denotes the solution when they included all their ADCP measurements (representing a snapshot). In terms of the section-averaged transport profiles, the model appears to compare reasonably well with the

	Model A11	Observed A11
Ekman transport (Sv)	5.68	4.9
Ekman heat transport (PW)	0.26	0.21
WBC (Sv)	24.2	45.0
Total heat transport (PW)	0.62	0.53
Overturning (PW)	0.42	0.35

Table 7: Heat transport across WOCE section A11.

preferred solution of Saunders and King (1995) with the southward flow a little deeper than the observations suggest and the northward flow of bottom water a little shallower than observations suggest. Saunders and King (1995) supported the idea of a warm water route[2] for supplying North Atlantic Deep Water partly because the net heat flux occurred within the subtropical gyre (that is to say the eastern half of the A11 section). Figure 7 shows the volume and heat fluxes accumulated from the western boundary across the A11 section in HadCM2. As in the observations the major contribution to the net heat flux arises near the eastern boundary which suggests that the model also supports the warm water route. Presumably the large momentum diffusion coefficient in the model allows a persistent westward flux to exist around Cape of Good Hope. This may however overestimate the export of Aghulas water from the Indian basin into the Atlantic basin which is usually believed to take place via the formation of Aghulas rings at the retroflection zone.

3.5 Indo-Pacific region

The Indo-Pacific is usually treated by modellers as one ocean, since the net mass transport across any section is then identical to zero and there will exist a well-defined heat transport. However, observational estimates usually consider the oceans independently and there are very few estimates where the Indian Ocean and South Pacific heat transports are estimated together consistently. It is for this reason that we consider the two oceans independently.

In the South Pacific, hydrographic estimates derive from the use of inverse models; at 17°S, Tsimplis *et al* (1996) estimate a southward heat transport of -0.36 PW, at 28°S, Wunsch *et al* (1983) estimate -0.18 PW and at 32°S, Tsimplis *et al* (1996) estimate -0.26 PW. The model temperature transports of 0.74 PW at 32°S and 0.66 PW at 17°S are clearly at variance with the observations. Other numerical models also transport temperature northward in the South Pacific (see for example,

[2]The warm water route (Gordon, 1986) is an idealistic circulation where the northward flow in the South Atlantic compensating for the southward export of North Atlantic Deep Water originates from the Indian Ocean, while in the cold water route (Rintoul, 1991) the northward flow originates from the Pacific Ocean and enters the South Atlantic via Drake Passage.

Latitude	Temperature transports			Adjusted heat transports		
	S. Pacific	Indian	Indo-Pacific	S. Pacific	Indian	Indo-Pacific
17°S	0.66	-1.83	-1.17	-0.15	-1.14	-1.29
32°S	0.74	-1.47	-0.73	0.08	-0.91	-0.83

Table 8: Temperature transports (converted to PW) with initial velocity fields and heat transports (PW) after velocity field in western boundary current regions are adjusted such that each section has zero net mass transport in South Pacific, Indian Ocean and combined Indo-Pacific.

Saunders and Coward (1996)) and this is often attributed to the net flow. However, the inverse calculations are not able to indicate a preferred magnitude for the net flow (Tsimplis *et al*, 1996). Barotropically adjusting the velocity fields in the western boundary current such that the net mass transport across the section is reduced to zero and the temperature transports become well-defined heat transports, leads to a reduction in the northward flux of temperature at both 17°S and 32°S as shown in table 8. The results suggest that much more satisfactory agreement between the model and observations will be reached with a lower magnitude of the Indonesian throughflow (see also section 3.1).

Across a latitude of 32°S in the Indian Ocean, all the observations show a southward transport of temperature but there is no common agreement on its magnitude. The most recent estimate of Toole and Warren (1993) is compared with the model results in table 9. Most of the apparent discrepancy may be due (as was the case in the South Pacific) to the assumed Indonesian throughflow (Toole and Warren (1993) assume a throughflow of 6.7 Sv while the model throughflow is 22 Sv). Adjusting the velocities in the western boundary current to imply zero mass transport, leads to a reduction in the southward flux of temperature at both latitudes (as seen in table 8). The implication of the adjustment for the combined Indo-Pacific region can now be assessed; at 32°S the adjustment increases the southward heat transport from -0.73 PW to -0.83 PW, while at 17°S, the adjustment increases the southward heat transport from -1.16 PW to -1.29 PW. This suggests that the adjustment introduces an error of order(0.1 PW) by combining the two basin heat transports. Also, since the flux divergence between sections in each ocean basin is not conserved during the adjustment, the method should be treated somewhat cautiously.

4 Global circulation

Figure 8 shows the global circulation diagnosed by Macdonald (1995) in temperature classes which broadly describe four water mass types: θ>7°C (surface), 7°C>θ>3.5°C (intermediate),

	Model 32°S	Observed 32°S
Ekman transport (Sv)	-0.7	1.6
Ekman heat transport (PW)	-0.06	0.12
Interior transport (Sv)	-22.3	-8.2
Interior heat transport (PW)	-1.41	-1.79
Total heat transport (PW)	-1.47	-1.67

Table 9: Heat transport across 32°S in the Indian Ocean. HadCM2 versus the observations of Toole and Warren (1993). There is a residual mass transport across both sections.

3.5°C>θ>1.8°C (deep) and θ<1.8°C (bottom). Figure 9 shows the circulation in HadCM2 diagnosed for the same temperature classes. In the surface layer of the model, most of the northward flow in the South Atlantic is supplied from the Indian Ocean. The observations suggest a much weaker exchange between the two oceans with over half of the northward flow of surface water in the Atlantic supplied by conversion of colder water masses and suggesting that the warm water path is enhanced in HadCM2. In fact, the diagnosis of HadCM2 suggests that there is one global circulation cell (a conveyor belt?) while the observations suggest that the Atlantic and Indo-Pacific are almost disparate (Macdonald, 1995).

In the intermediate and deep layers, the differences between the model and observations are dominated by the southward export of NADW in the Atlantic which takes place in the intermediate layer in the model and in the deep layer in observational estimates. This was discussed in more detail earlier in this report. The deep water circulation is broadly similar in both schematics except for a weakened northward flow in the model in both the Indian and the North Pacific Oceans. A further comment regards the strength of the Antarctic Circumpolar Current, which has a magnitude of 141 Sv in the observations and 218 Sv in the model. This is typical of many Cox models but requires further investigation.

5 Conclusions

Here we have examined the heat transport in a coupled model which employs flux correction. In the northern oceans the model typically underestimates the northward heat transport when compared with observations. In contrast, in the southern hemisphere the South Atlantic shows remarkable agreement with observational estimates. The model errors identified from this analysis can be summarised:

- the deep southward flow in the North Atlantic is too shallow. This may be related to the poor representation of the overflows already identified by Roberts *et al* (1996).

- the thermocline is too diffuse, particularly in the North Pacific. This may be improved by the implementation of the eddy mixing scheme of Gent and McWilliams (1990).

- the magnitude of the Indonesian throughflow lies outside the acceptable observational range and the implications of the magnitude of the throughflow on the heat budget of the region need to be investigated further. In particular, it is still unclear how to define independent heat transports in the Pacific and Indian Oceans.

- the link between the Atlantic and Indian oceans appears to be much stronger in HadCM2 than is indicated by the observations. This may be due to the large momentum diffusion coefficients which are required by the coarse resolution.

As the oceanographic community move into the analysis and interpretation phase of WOCE, more robust estimates of heat transport will become available for the southern hemisphere. Validation of the ocean component of HadCM2 and its successors will then have a more global extent than is presently possible.

References

Bryden, H. L., D. H. Roemmich, and J. A. Church, 1991: Ocean heat transport across 24°N in the Pacific. *Deep-Sea Research*, **38**, 297–324.

Fu, L.-L., 1981: The general circulation and meridional heat transport of the subtropical South Atlantic determined by inverse methods. *Journal of Physical Oceanography*, **11**, 1171–1193.

Gent, P. R., and J. C. McWilliams, 1990: Isopycnal mixing in ocean circulation models. *Journal of Physical Oceanography*, **20**, 150–155.

Gordon, A. L., 1986: Interocean exchange of thermocline water. *J. Geophys. Res.*, **91**, 5037–5046.

Hall, M. M., and H. L. Bryden, 1982: Direct estimates and mechanisms of ocean heat transport. *Deep-Sea Research*, **29**, 339–359.

Johns, T. C., R. E. Carnell, J. F. Crossley, J. M. Gregory, J. F. B. Mitchell, C. A. Senior, S. F. B. Tett, and R. A. Wood, 1997: The second Hadley Centre Coupled Ocean-Atmosphere GCM: Model description, spinup and validation. *Climate Dynamics*, **13**, 103–134.

Macdonald, A. M., and C. Wunsch, 1996: Oceanic estimates of global ocean heat transport. *US WOCE Report*, 28–30.

——, 1995: *Oceanic fluxes of mass, heat and freshwater: A global estimate and perspective*. PhD thesis, MIT/WHOI.

Rintoul, S. R., 1991: South Atlantic interbasin exchange. *J. Geophys. Res.*, **96**, 2675–2692.

Roberts, M. J., R. Marsh, A. L. New, and R. A. Wood, 1996: An intercomparison of a Bryan-Cox-type model and an isopycnic ocean model. Part I: The subpolar gyre and high-latitude processes. *Journal of Physical Oceanography*, **26**, 1528–1551.

Saunders, P. M., and A. C. Coward, 1996: An investigation and validation of a global ocean model (OCCAM). *WOCE International Newsletter*, **24**, 7–9.

——, and B. A. King, 1995: Oceanic fluxes on the WOCE A11 section. *Journal of Physical Oceanography*, **25**, 1942–1958.

Toole, J. M., and B. A. Warren, 1993: A hydrographic section across the subtropical south Indian Ocean. *Deep-Sea Research*, **40**, 1973–2019.

Tsimplis, M., S. Bacon, and H. Bryden, 1996: Heat fluxes of the south Pacific estimated through inverse models. *WOCE International Newsletter*, **24**, 10–12.

Wijffels, S. E., N. Bray, S. Hautala, G. Meyers, and W. Morawitz, 1996: The WOCE Indonesian throughflow repeat hydrography sections: I10 and IR6. *WOCE International Newsletter*, **24**, 25–28.

Wunsch, C., D. Hu, and B. Grant, 1983: Mass, heat, salt and nutrient fluxes in the south Pacific Ocean. *Journal of Physical Oceanography*, **13**, 725–753.

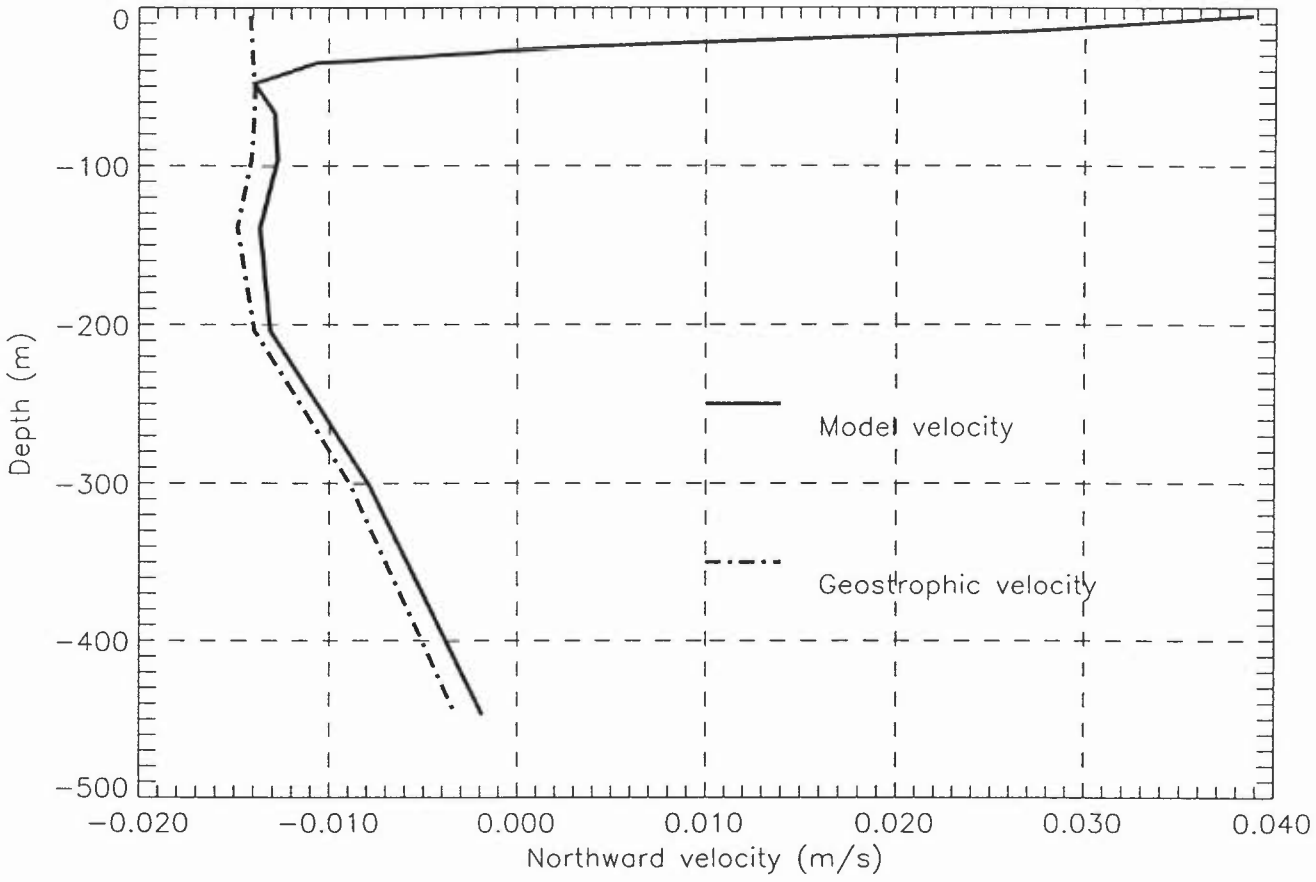

Figure 1: Model velocity profile (bold) and geostrophic velocity profile (dashed) (calculated from model density) for 150°E, 24°N. The geostrophic velocity has been matched to the model velocity at a depth of 50 m.

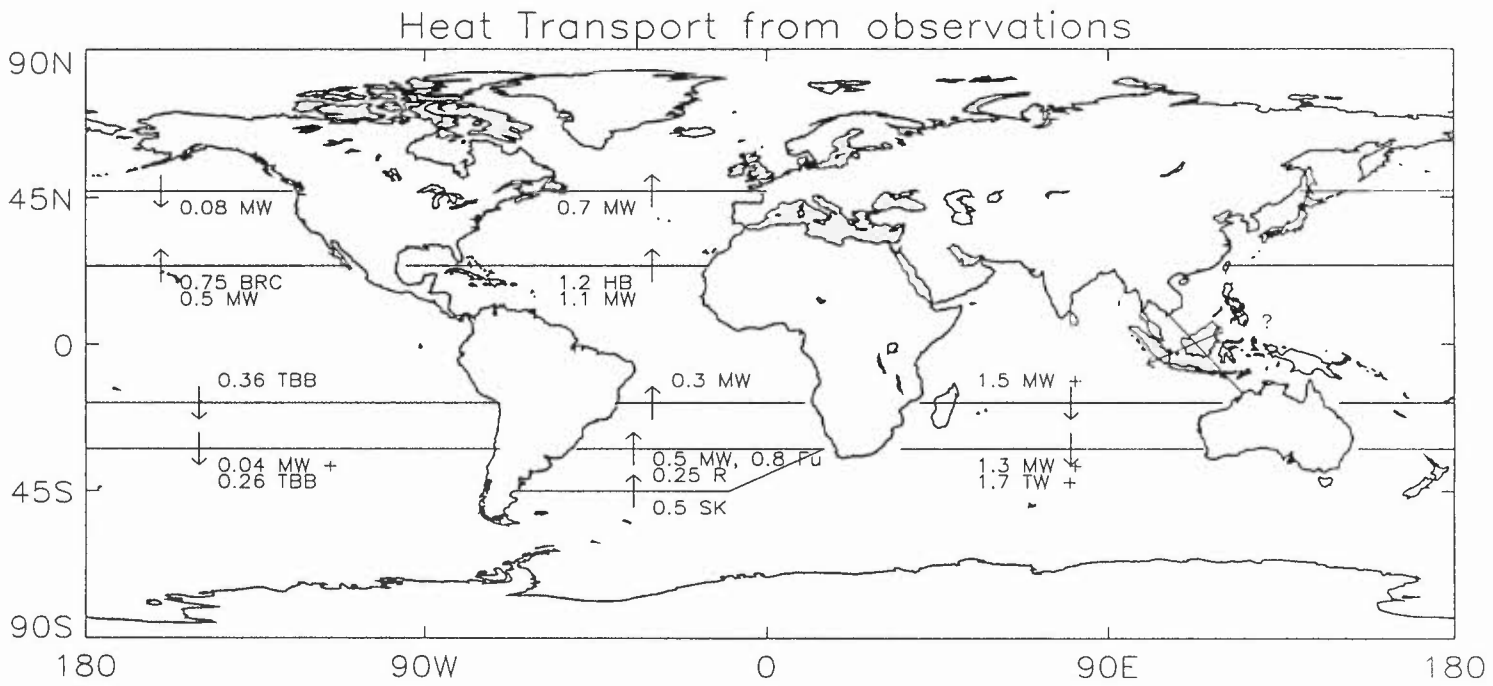

Figure 2: Heat transport (PW) estimated from observations across the marked sections in the direction indicated by the arrows. The daggers indicate that the estimate includes a non-zero mass flux across the section. The initials denote the authors; MW is Macdonald and Wunsch (1996), BRC is Bryden *et al* (1991), HB is Hall and Bryden (1982), TBB is Tsimplis *et al* (1996), Fu is Fu (1981), R is Rintoul (1991), TW is Toole and Warren (1993) and SK is Saunders and King (1995).

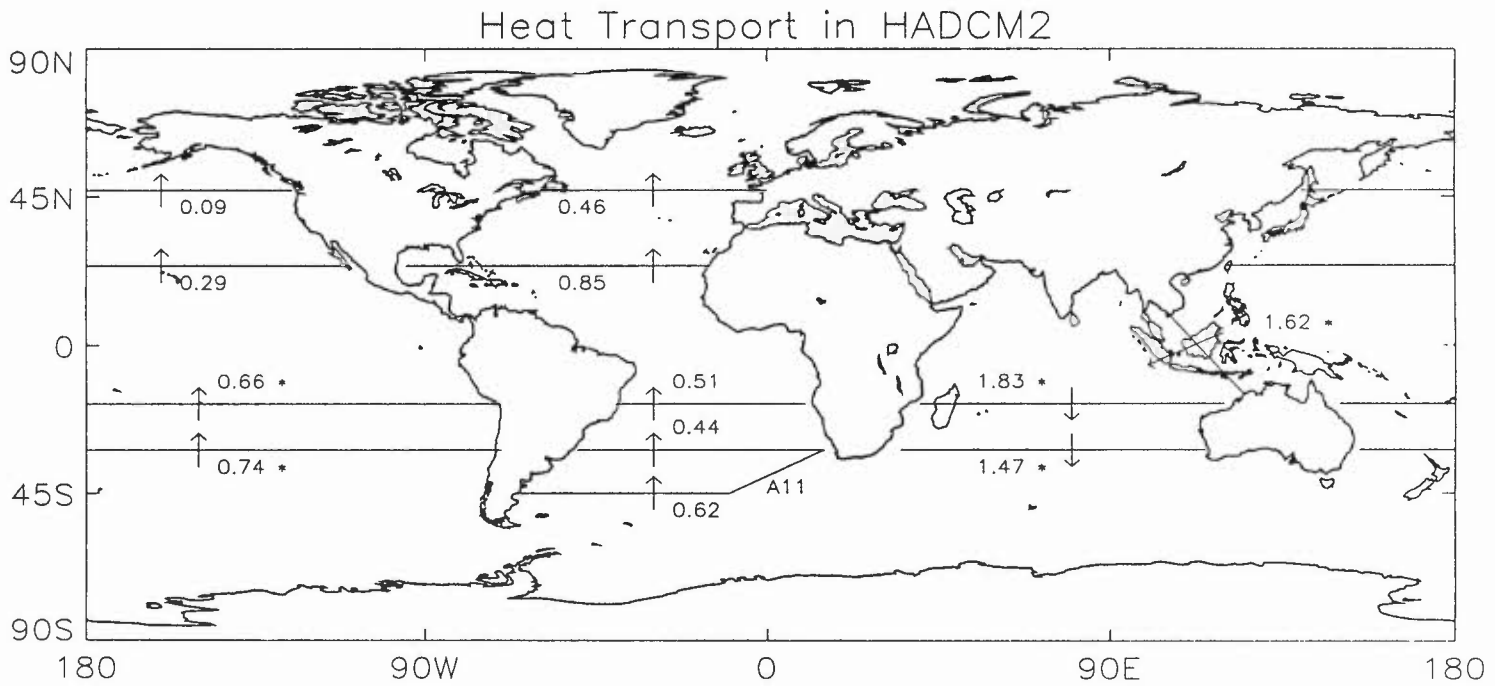

Figure 3: Heat transport (PW) in HADCM2 across marked sections in the direction indicated by arrows. The asteriks indicate that the mass transport is non-zero across the marked section and the quantity indicated is a temperature flux.

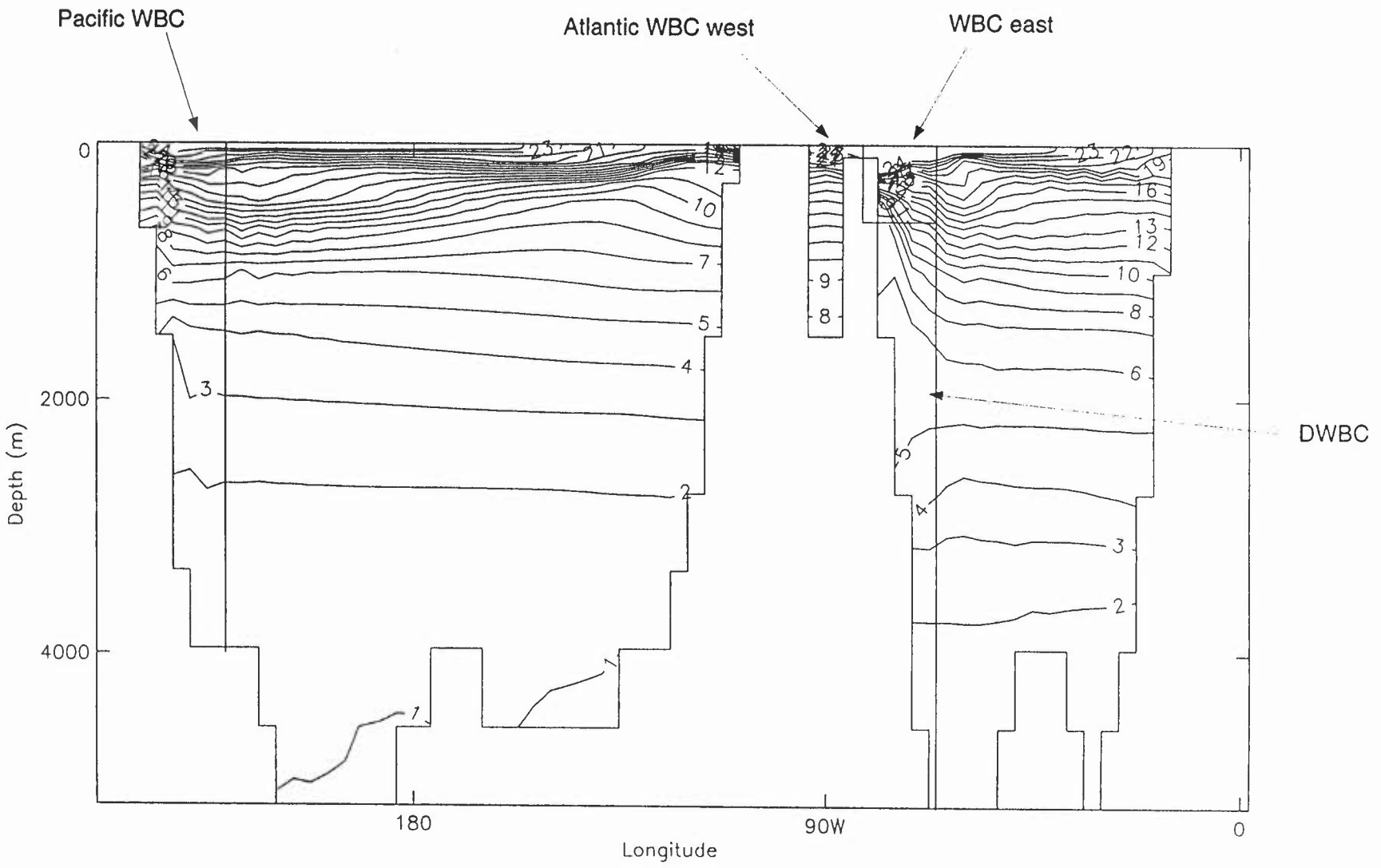

Figure 4: Potential temperature (°C) across 24°N in HADCM2. Marked on the section are the limits of the western boundary currents (WBC) and (in the Atlantic) deep western boundary current (DWBC).

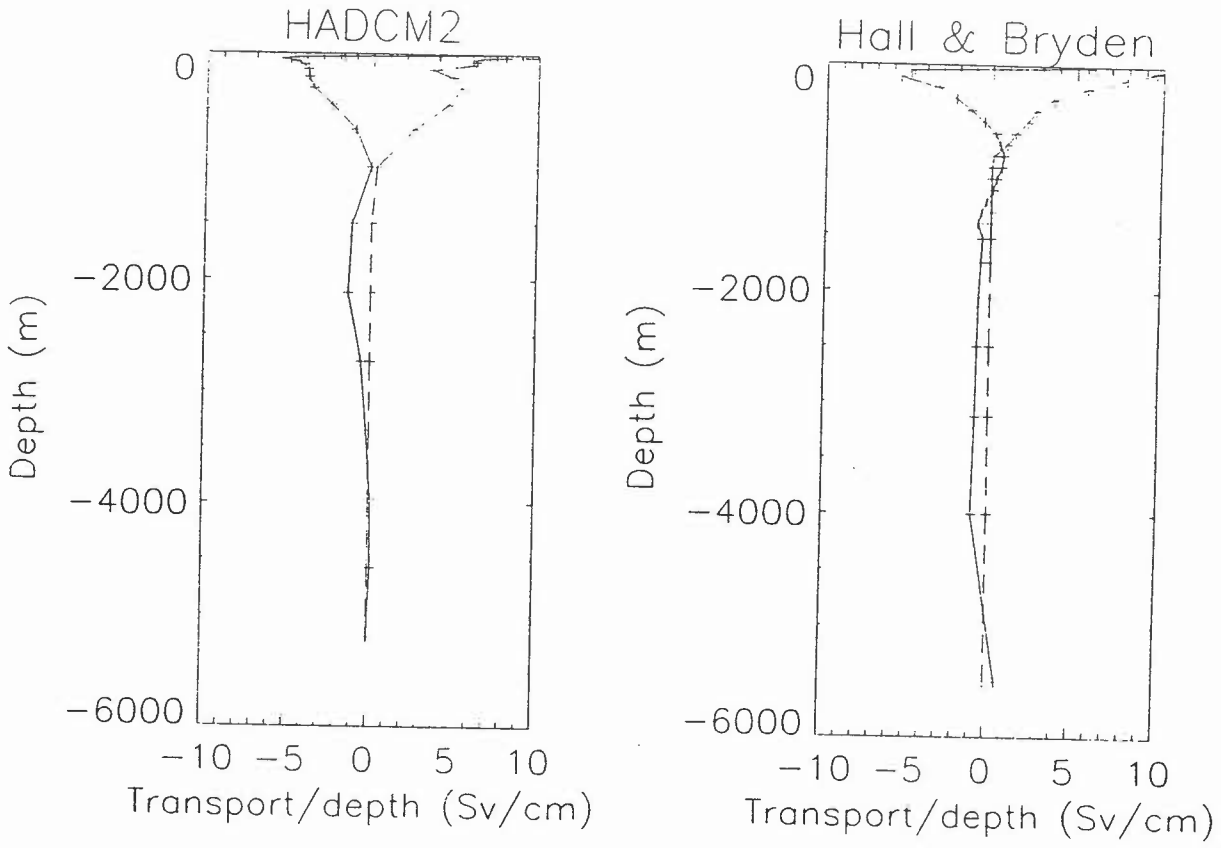

Figure 5: Transport per unit depth across Atlantic 24°N section for HADCM2 and the observations of Hall and Bryden (1982). The dashed line indicates the western boundary current contribution and the bold line indicates the interior plus Ekman contribution.

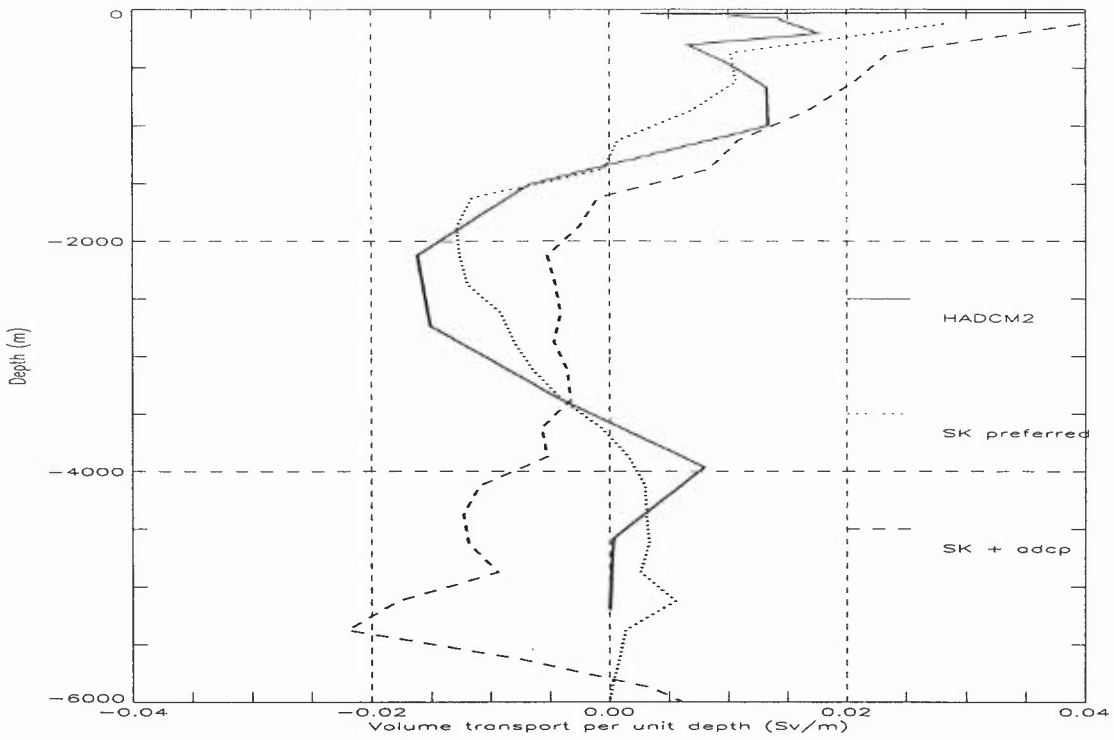

Figure 6: Transport per unit depth across WOCE section A11 for HADCM2 and the observations of Saunders and King (1995).

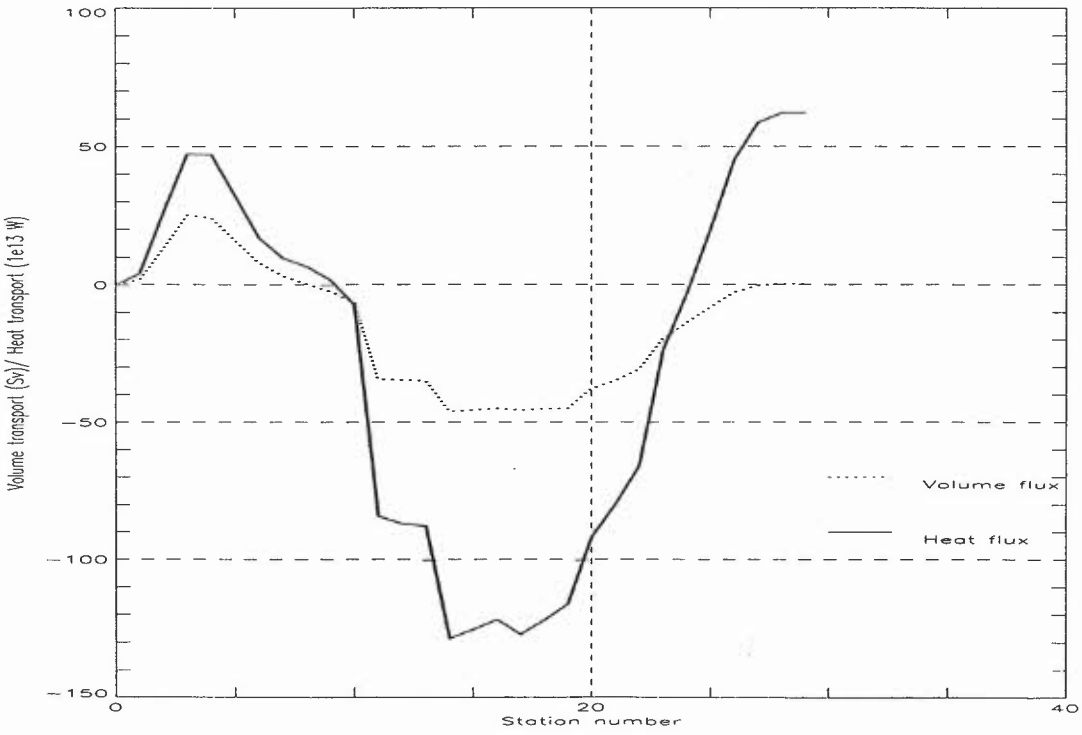

Figure 7: Cumulated heat and volume transport from the western boundary across the A11 section.

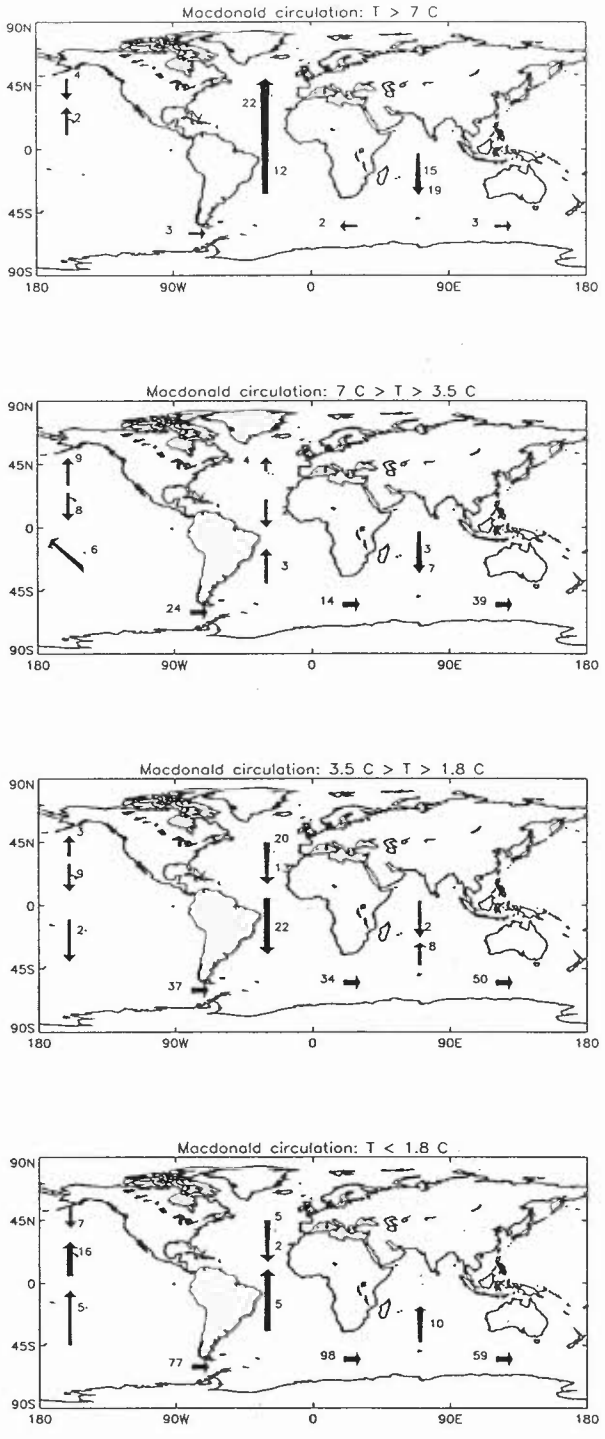

Figure 8: The global circulation estimated by Macdonald (1995) for the four temperature classes; $\theta > 7°C$ (surface water), $7°C > \theta > 3.5°C$ (intermediate water), $3.5°C > \theta > 1.8°C$ (deep water) and $\theta < 1.8°C$ (bottom water). The arrows are not to scale.

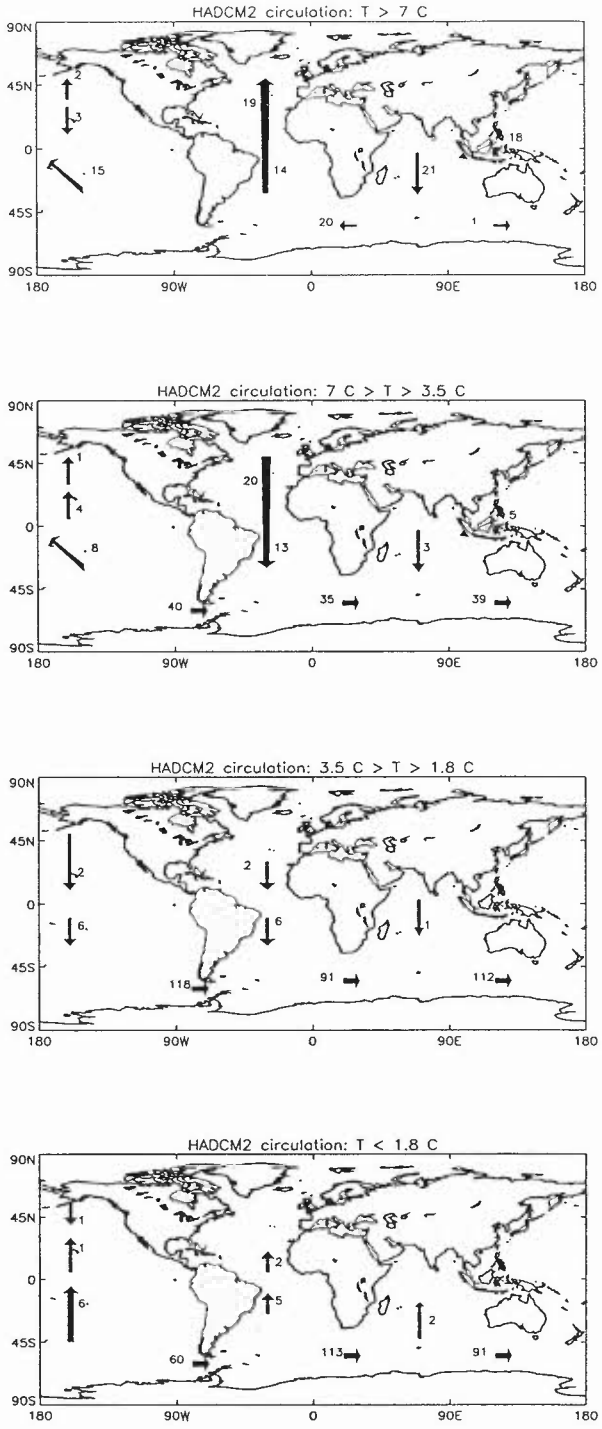

Figure 9: The global circulation calculated for HADCM2 for the four temperature classes; $\theta > 7°C$ (surface water), $7°C > \theta > 3.5°C$ (intermediate water), $3.5°C > \theta > 1.8°C$ (deep water) and $\theta < 1.8°C$ (bottom water). The arrows are not to scale.